Chemical Physics 398 (2012) 176–185

Contents lists available at ScienceDirect

Chemical Physics

journal homepage: www.elsevier.com/locate/chemphys

On the role of charge transfer in the stabilization of weakly bound complexes involving water and hydrogen sulphide molecules

F. Pirani [a], P. Candori [b], M.S. Pedrosa Mundim [a,c], L. Belpassi [a,d,*], F. Tarantelli [a,d], D. Cappelletti [b,*]

[a] Dipartimento di Chimica, Università di Perugia, 06123 Perugia, Italy
[b] Dipartimento di Ingegneria Civile e Ambientale, Università di Perugia, 06125 Perugia, Italy
[c] Instituto de Fisica, Universidade Federal de Bahia, 40000 Salvador Bahia, Brazil
[d] ISTM-CNR, 06123 Perugia, Italy

ARTICLE INFO

Article history:
Available online 9 April 2011

Keywords:
Hydrogen bond
Charge transfer

ABSTRACT

Integral cross section data for collisions of water and hydrogen sulphide molecules with noble gas atoms, measured with the same apparatus under identical conditions and analyzed by exploiting the same potential model, provided a set of internally consistent potential parameters. Their critical comparison is exploited not only to identify those systems where the intermolecular bond is not simply due to the balancing of size repulsion with dispersion and induction attraction, but also to establish the amount of bond stabilization by charge-transfer effects. Such experimental findings are analyzed through extensive and accurate ab initio calculations, addressed at discovering the relevant differences in the basic features of the potential energy surfaces. In particular, we have analyzed in detail the prototype H_2S, H_2O–Kr systems and found pronounced differences in the dependence of the interaction nature and energy on the relative orientation of the colliding systems. Using the recently proposed charge-displacement analysis we have been able to quantitatively assess charge-transfer effects, which differ significantly in the two systems and exhibit different stereoselectivity. This casts further light on the specificity of water interactions.

1. Introduction

The study of intermolecular forces represented for a long time a fundamental and broad field of research [1,2] with key issues relevant for both basic and applied science. A fascinating case of study concerns the formation of the hydrogen-bond (H-bond) which, because of its relevance for the description of water properties in several environments and of biological systems, has been persistently the target of many experimental and theoretical investigations (see for instance Ref. [3]).

One basic aim of this research, which is also the focus of the present work, is to work out a correct partition of the intermolecular forces involved and to establish the nature of the various interaction contributions. Among others, the role of charge transfer (CT) contribution to the stabilization of H-bonded structures is one of the most interesting and debated issues (see for example Refs. [4–10]). The effort to identify and characterize these contributions is mandatory in order to develop models founded on solid grounds and useful for the description of force fields operative in complex systems of applicative interest. To this aim, the combination of high resolution experiments and detailed theoretical investigations represents the more effective approach.

Not long ago, we demonstrated, by performing high resolution molecular beam scattering experiments and analyzing the measured cross sections [11], that the water–noble gas complexes cannot be classified as conventional non-covalent systems, i.e. bound by the simple balancing of size repulsion with dispersion and induction attraction, because the presence of an appreciable (i.e. measurable) charge transfer stabilization contribution [12]. The latter, somehow unexpected for such closed shell interacting particles, was demonstrated to be stereoselective, showing the maximum strength for the noble gas approaching water on the hydrogen side and rapidly vanishing with the intermolecular distance [12,13]. Moreover, since a charge amount of few millielectrons is transferred from the noble gas towards the water molecule, as elucidated from electron density calculations [12], the experimentally observed increasing stabilization of the heavier noble gas–water complexes was correlated to the decrease of the ionization potential [13]. We stress that establishing these correlations between interaction components and basic atomic and molecular properties is very important for the modeling of intermolecular forces in complex systems, and can only be achieved by investigating in detail relatively simple systems both experimentally and theoretically.

* Corresponding authors. Fax: +39 0755853864 (D. Cappelletti).
E-mail addresses: belp@thch.unipg.it (L. Belpassi), david.cappelletti@unipg.it (D. Cappelletti).

0301-0104/$ - see front matter © 2011 Elsevier B.V. All rights reserved.
doi:10.1016/j.chemphys.2011.03.030

Recently [14],we have also studied in detail the water–H_2 system, for which an electrostatic component (due to permanent dipole–permanent quadrupole interaction) is operative. A significant and far more intriguing stereoselectivity of the charge transfer was discovered for this prototype molecular complex. In particular, when the hydrogen molecule approaches water from the side of its hydrogen atoms, with its axis perpendicular to the water plane, some millielectrons are transferred from H_2 towards H_2O as in the noble gas case. But when the hydrogen molecular axis is pointed towards the oxygen atom along the C_{2v} symmetry axis of water, the reverse effect occurs, with water acting as an electron donor. Namely, we observed in embryo the acid–base character of water.

In this paper we further characterize this interesting phenomenon, elucidating in greater detail its stereospecificity and the role of the molecular electron acceptor. In particular, we exploit the comparison of the integral cross section, Q, for the scattering of water and hydrogen sulfide by noble gas atoms, recently measured [11,13,15,16] under the same experimental conditions, as a function of the collision velocity v. In all cases, except for He, a neat oscillatory pattern associated to the glory quantum interference effect was observed, superimposed to a smooth decreasing average component. These observables depend on the absolute scale of the intermolecular interaction in the well region and at long range, respectively [17]. Moreover, the analysis of $Q(v)$, carried out exploiting a recently proposed model potential which involves only two parameters, provided a set of potential parameters useful to describe in a unifying and internally consistent way both the asymptotic region of the attraction and the potential well of all systems [17]. Such $Q(v)$ data can be also compared with cross sections for the corresponding (i.e. similar) noble-gas–noble-gas systems, for which an accurate description of the interaction in terms of the same potential model has been recently proposed by analyzing data of the same type [17].

Furthermore, a detailed comparative coupled-cluster theoretical study is presented for the specific case of water and hydrogen sulfide interacting with the krypton atom. Several relevant sections of the potential energy surface (PES) for the interaction between H_2S and Kr have been computed and are discussed in detail, along with the determination of the most stable nuclear configuration determined by full geometry optimization. An illuminating detailed comparison is carried out with the corresponding properties of the H_2O–Kr adduct. A key aspect of the work is the quantitative analysis of the charge displacement taking place upon formation of the adducts which, as already amply demonstrated [18,12–14] is extremely useful to characterize the different role of charge transfer.

Section 2 reports a short description of the experimental framework used in the scattering measurements and summarizes the results of their analysis. A critical internal comparison of the obtained potential parameters is carried out in Section 3. The computational details and analysis the results of geometry optimizations and their energetics will be presented in Section 4. Finally, in Section 5, we will be discussed the charge displacement effects.

2. Scattering experiments and their analysis

The subjects of this section are important to shortly recall the main conditions used during the measurements and then to define type and amount of information obtainable from the analysis of the experimental data. The experimental apparatus used to perform the scattering experiments consists of a set of differentially pumped vacuum chambers connected by slits for the molecular beam (MB) collimation. MB emerges through a nozzle (1 mm in diameter), from a source which can operate under nearly effusive or moderately supersonic conditions. After mechanical velocity selection, MB crosses a scattering chamber, which can be cyclically filled and emptied with the target gas by an automated procedure (total period 20 s, duty cycle 50%). After the scattering region, the on-line beam intensity is detected by an electron bombardment ionizer followed by a quadrupole mass spectrometer. The MB velocity analysis and selection is obtained with the use of a slotted disk velocity selector with a high resolution (full width at half maximum less than 5%). The measurement of the MB attenuation I/I_0 (were I and I_0 represent the MB intensity with and without target gas in the scattering chamber) at each selected MB velocity v, permits the determination of the integral cross section $Q(v)$ as a function of the velocity v, through the Lambert–Beer law.

$$Q(v) = -\frac{1}{NL}\log\frac{I}{I_0}, \tag{1}$$

where N is the target gas density and L the effective length of the path in the scattering chamber. All the geometrical characteristics and details of the apparatus are given elsewhere [19].

Water MBs have been generated by expansions of water vapor through a nozzle heated to 500–600 K, in order both to suppress cluster formation and to "heat up" the rotational motion of the molecular species. 100% isotopically substituted D_2O has been employed to take advantage of the fact that the background noise in the mass spectrometer is much smaller at $m/e = 20$, with respect to that at $m/e = 18$. D_2O vapor has been kept in the source both pure, at a stagnation pressure of 5 mbar, and in a mixture with H_2 always at low stagnation pressure, in order to cover a wide collision velocity range [11,13]. Similar source conditions have been exploited in order to produce H_2S MBs [15,16]. The scattering chamber has been kept at the liquid air temperature ($\sim$90K), in order to enhance the velocity resolution of the experiments. As previously [20–22], the absolute values of $Q(v)$ have been obtained by an internal calibration of the NL factor based on the direct measurement of the gas flow in the scattering chamber and on the absolute values of the He–Ar cross sections [23].

The MBs, generated from hot sources, contain molecules that rotate sufficiently fast during each collision to exploit essentially elastic events, mostly driven by the average (isotropic) interaction component [19,20,24,25].

$Q(v)$ data for water and hydrogen sulphide interacting with the same noble gas atom can be directly compared since measured under the same conditions. Fig. 1 reports $Q(v)$ measured for both projectile molecules colliding with Kr and emphasizes that such data exhibit similar velocity dependence, while for H_2S–Kr the absolute scale of $Q(v)$ is 30% larger. Such a comparison indicates that while the long range attraction for H_2S–Kr is about a factor two larger with respect to that of H_2O–Kr, the strength of the interaction in proximity of the minimum of the potential well is comparable. Difference and similarity in the interactions, analyzed here in the specific case of Kr, has been observed in all the other systems involving the same noble gas (Ng) atom.

A direct and quantitative comparison of the potential features can be made only if the considered observables are all of the same type and they are analyzed by using the same potential function parameterized in a reliable way. For such a reason the analysis has been performed, in all systems, by using the ILJ (improved Lennard–Jones) model [17,26], whose functional form is the following

$$V(r) = \varepsilon\left[\frac{6}{n(r)-6}\left(\frac{r_m}{r}\right)^{n(r)} - \frac{n(r)}{n(r)-6}\left(\frac{r_m}{r}\right)^{6}\right], \tag{2}$$

where

$$n(r) = \beta + 4\left(\frac{r}{r_m}\right)^2. \tag{3}$$

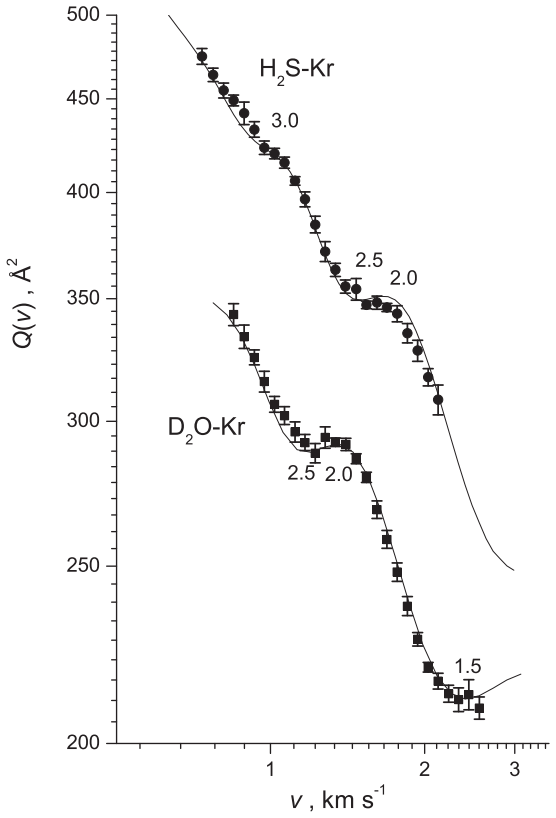

Fig. 1. Cross sections Q for the D_2O–Kr and H_2S–Kr systems, plotted as function of the beam velocity v. Symbols are the experimental data and lines are the fits using the ILJ potential model (see text). Numbers indicate the glory extrema order.

In Eq. (2) the first term represents the repulsion while the second one the attraction. The ε parameter defines the depth of the potential well, r_m fixes the equilibrium distance and β, associated to the hardness of the involved chemical species, determines the shape of the potential in the region of the well. We have taken [13,27] $\beta = 9$, a value typical of weak intermolecular interactions between neutral species [17].

During the fitting procedure of experimental data both ε and r_m have been varied, in order to properly reproduce amplitude and position of the observed glory extrema and the absolute value of $Q(v)$, the latter within the uncertainty of its calibration (3%–4%). The cross sections $Q(v)$, calculated in the center of mass frame, assuming a defined $V(r)$ and using the JWKB method for the phase shift, have been convoluted in the laboratory system for the direct comparison with the experimental data. All the involved potential parameters have been reported in Refs. [13,27].

From the above analysis, a long–range attraction coefficients C_6 can be also predicted by Eq. 2 (for $r \to \infty$, $C_6 \to \varepsilon r_m^6$). As in [13,16,17] the C_6 coefficient, so obtained from the best fit parameters, includes both dispersion and induction contributions, i.e. $C_6 = C_{disp} + C_{ind}$. In order to separate the relative contribution of the two terms, we make use of polarizabilities (α) and permanent dipole moments (μ) of the interacting partners (see Table 1). In particular, as detailed in the next sections, the long–range induction coefficient can be evaluated as $C_{ind} \sim \alpha\mu^2$ and the dispersion coefficient C_{disp} can be predicted on the basis of the venerable Slater–Kirkwood approximation, as described in Ref. [28]. In this way we can estimate $C_{ind}/C_{disp} \sim 0.10$ for the H_2O–Kr, $\sim$ and $\sim$0.02 for H_2S–Kr. Such ratios were useful [13,16] to separate induction and dispersion contributions to the C_6 coefficient for all water, hydrogen sulphide–noble gas systems.

Table 1
Polarizability (α) and dipole moment (μ) of the interacting molecular species.

	α (Å^3)	μ (D)
Water	1.47	1.85
Hydrogen sulfide	3.78	0.98
Argon	1.64	
Xenon	4.04	

1 D = 3.336 × 10^{-30} C m and 1 Å = 0.1 nm.

3. A critical comparison of the potential parameters

As previously stressed by us in [12,13], for water–Ng systems the features of the van der Waals interaction, defined by us for convenience as arising from the balancing of size repulsion with dispersion attraction, are expected to be very similar to that in the corresponding Ar–Ng dimers. This correspondence is suggested by the closeness of the average polarizability value of water and argon (see Table 1) which is the basic property controlling the van der Waals interaction [28]. Note also that, under the conditions of these experiments (rotationally hot MB), the induction contribution, due to permanent dipole–induce dipole attraction and operative in the water–Ng systems, exhibits a small effect along the Ng series. Moreover, the induction to dispersion ratio is approximately constant for all the water–Ng complexes. Such attenuated contribution tends to compensate small effects due to the difference in water and Ar polarizability value (see again Table 1). For the same reasons it is meaningful to compare H_2S–Ng and Xe–Ng systems (see Table 1 and [16]).

The Fig. 2 compares the scattering observable for the four systems involving Kr. We note that while the smooth component of $Q(v)$ differs in only 3% for H_2O–Kr and Ar–Kr and in 5–6% (again within the mutual experimental uncertainty) for H_2S–Kr and Xe–Kr systems, the glory pattern exhibits a well evident shift and different sign. However, we can now compare directly also the basic features of all the intermolecular potentials, since obtained by the internally consistent procedure described above.

We have summarized such a critical comparison in Figs. 3 and 4, where the experimentally determined ratios concerning the potential well (ε) and the long range attraction coefficient (C_6) (water–Ng respect to Ar–Ng and hydrogen sulphide–Ng respect to Xe–Ng) are reported respectively as a function of the polarizability

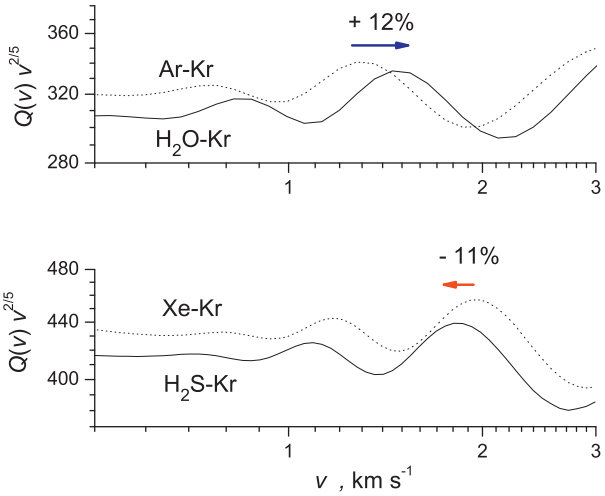

Fig. 2. Cross sections Q for the H_2O–Kr and H_2S–Kr systems, and the analogous Ar–Kr and Xe–Kr rare gas dimers, as a function of the beam velocity v. The cross sections are plotted as $Q \cdot v^{2/5}$, in order to emphasize the glory structure.

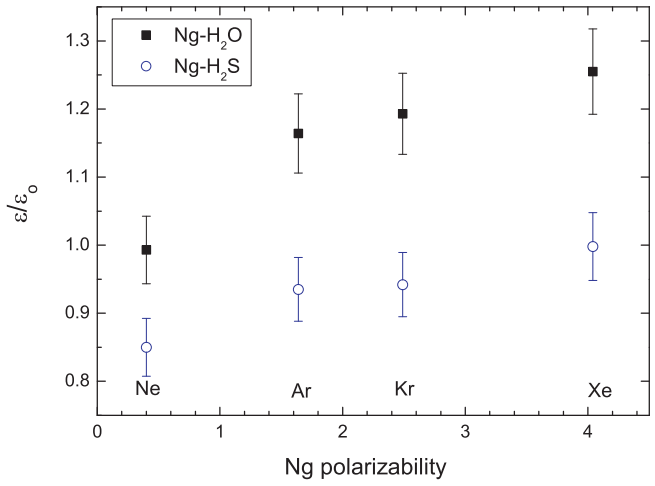

Fig. 3. Experimental ratio of the potential well ε for H_2O–Ng and H_2S–Ng complexes to that ε_0 of the corresponding Ar–Ng and Xe–Ng systems respectively, plotted as a function of the polarizability of Ng.

of Ng. As can be seen, while the C_6 coefficient scales in a very similar way, the potential well ε deepens increasingly for both molecule–Ng systems along the Ng family and in a more pronounced way for water–Ng. Therefore, such a comparison indicates that a component, additional to the combination of van der Waals with induction, tends to be more stabilizing in going towards the heavier noble gas and emerges in a more pronounced way for systems involving water. The experimental findings summarized in Figs. 2–4 also suggest that such additional component must be effective at intermediate intermolecular distances (i.e. in the neighborhood of the potential well) and must vanish at large intermolecular distances. We have attributed such additional stabilization to a charge transfer component which is expected to be related to the overlap of outer molecular clouds and whose amount strongly varies with the distance. Moreover, exploiting the interaction of the reference Ng–Ng systems, we can obtain, in absolute scale and at the equilibrium distance, the bond stabilization due to such additional component, except for cases with He for which the effect is less pronounced, the glory pattern has been not observed and experimental determinations are less accurate. In particular, we have exploited the deviations of the potential well depth ratio from 1

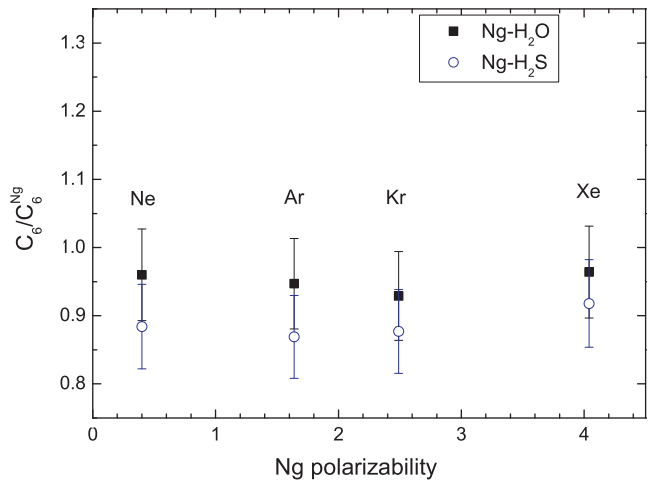

Fig. 4. Experimental ratios of long range attraction coefficients (C_6) for H_2O–Ng and H_2S–Ng complexes to that (C_6^{Ng}) of the corresponding Ar–Ng and Xe–Ng systems respectively, plotted as a function of the polarizability of Ng.

Table 2
Estimated bond stabilization $\delta\varepsilon$ in meV (see text).

System	$\delta\varepsilon$ (meV)
H_2O–Ne	0.0 ± 0.3
H_2O–Ar	2.0 ± 0.6
H_2O–Kr	2.8 ± 0.7
H_2O–Xe	4.1 ± 0.8
H_2S–Ne	0.0 ± 0.3
H_2S–Ar	1.4 ± 0.8
H_2S–Kr	1.9 ± 0.9
H_2S–Xe	3.6 ± 1.2

and from 0.85 (see Figs. 3 and 4) for water–Ng and for hydrogen sulphide–Ng systems, respectively, to obtain the absolute value of the stabilization $\delta\varepsilon$. Results (see Table 2) show that $\delta\varepsilon$ is larger for the water–Ng systems with respect to the analogous H_2S cases, although the values are within the estimated uncertainties. These findings are also consistent with those obtainable as difference between potential parameters experimentally determined and predictions of correlation formulas [28], proving ϵ and r_m for van der Waals interaction perturbed by the induction [12,27]. It should be noted that in the case of H_2S the CT component adds to a stronger van der Waals interaction and makes its experimental characterization more difficult.

Extensive theoretical calculations, addressed to an accurate description of the involved potential energy surface and a detailed investigation of the electron density modifications, has been exploited to confirm such suggestions provided by the analysis of $Q(v)$ experiments. Moreover, such theoretical efforts will be also important to establish the stereospecificity of such additional component. The theoretical analysis is presented in the following.

4. Theoretical calculations

4.1. Computational details

The calculations have been carried out at the coupled cluster level of theory [29–31] with single, double (CCSD), and perturbatively included triple excitations (CCSD (T)) using augmented correlation consistent polarized valence basis sets up to quintuple-zeta (aug-cc-pVxZ,with x = D, T, Q, 5) [32–34]. The program MOLPRO has been used throughout [35]. The interaction with the noble gas leaves the geometry of H_2S essentially unaffected and the change in the interaction energy due to H_2S geometry relaxation is negligible. The H_2S molecule has thus been kept rigid at its free equilibrium structure [36] during the geometry optimizations. The H–S distance is 1.33 Å and the H–S–H angle is 92.2°. The corresponding values derived by the ab initio potential energy surface of Tarczay et al. [37] or reported more recently by Varandas and Song [38] are in close agreement. All our computed energies have been corrected for the basis set superposition error (BSSE) evaluated using the counterpoise correction of Boys and Bernardi [39].

We have taken into consideration several profiles of the potential energy surface of H_2S–Kr, characterized by different relative orientations of the partners. We have investigated in detail the basis set convergence for the determination of both the equilibrium geometry of the complex and the corresponding interaction energy. We also present a comparative study of the potential energy profiles obtained for the H_2S–Kr and H_2O–Kr complexes. The detailed nature of the interaction and, in particular, the extent of the charge transfer between the H_2S (H_2O) molecule and Kr has been investigated on the basis of the analysis of the charge dis-

placement curves. Such analysis, summarized briefly later on, appears to be crucial to rationalize the main experimental findings presented in the previous section.

4.2. Geometry optimizations and interaction energies

The experimental and theoretical information on the structure and most stable configurations for H_2S–Ng is scarce (see the introduction of Ref. [15] and references therein). In particular for the H_2S–Kr complex system, the potential energy surface, most stable geometry and interaction energy are not available. We therefore start our study analyzing several different cuts of the PES for H_2S–Kr in order to locate the most stable nuclear configurations and to identify with accuracy the absolute minimum of the PES. With frozen-geometry fragments, the structure of the H_2S–Kr complex may be easily specified by three coordinates, one distance r and two angles Φ and Θ. r is the distance between Kr and sulfur (Kr–S) (the center of mass of H_2S almost coincides with S), Φ is the angle between the Kr–S axis and the C_2 symmetry axis of H_2S, with $\Phi = 0$ corresponding to Kr lying on the hydrogen side of the C_2 axis. Finally, Θ is the dihedral angle between the H_2S plane and the plane containing the C_2 axis and the Kr atom (with $\Theta = 0$ when the four atoms are all coplanar). Note that Θ is undefined when $\Phi = 0$ or $\Phi = 180$. We have investigated three different sections of the PES characterized by different values of the angle Θ, namely $\Theta = 0$, $\Theta = 45$, $\Theta = 90°$. We refer to $\Theta = 0$ as the *coplanar* configuration, to $\Theta = 90$ as the *perpendicular* configuration, and to $\Theta = 45$ as the *bisecant* configuration. In each configuration, the PES section investigated corresponds to varying Φ from 0° to 180° and re-optimizing r (i.e. minimizing the energy with respect to r) at each Φ value. The results, obtained at the aug-cc-pVQZ/CCSD (T), are reported in Fig. 5. The interaction energies are corrected for the BSSE. Note that, with our definition of the coordinate system the three cuts of the PES meet at a single nuclear configuration for $\Phi = 0$ and $\Phi = 180$. Therefore, each energy pattern represents a minimum energy walk (for fixed Θ) joining these two nuclear configurations. The Fig. 5 shows that for small angles of approach Φ the interaction energies are comparable. The interaction energy is about 22 meV for the common local minimum at $\Phi = 0$. As Φ increases to 40°–50° the three profiles exhibit a different behavior. In this region, the coplanar configuration ($\Theta = 0$) has a local maximum, the perpendicular configuration ($\Theta = 90$) shows a flex while a local minimum is found the bisecant section ($\Theta = 45$). Note however that, despite these qualitative differences, the three configurations lie within only about 3 meV from each other. As Φ further increases their energy patterns start to differ more significantly. The coplanar configurations are clearly the most stable and a deep minimum, which is in fact the PES absolute minimum (see below), is indeed found for such an arrangement, at an angle Φ of about 110°. The interaction energy here is 24.7 meV. Note that the perpendicular profile, at about at the same angle Φ, presents on the contrary a maximum, with an interaction energy 10 meV smaller. For larger values of the angle Φ the interaction energy increases and decreases monotonically for the perpendicular and coplanar configuration, respectively, finally coinciding at $\Phi = 180$ with a value of about 16.4 meV. The bisecant section shows clearly the smallest dependence on the angle of approach Φ, with a relatively flat energy profile.

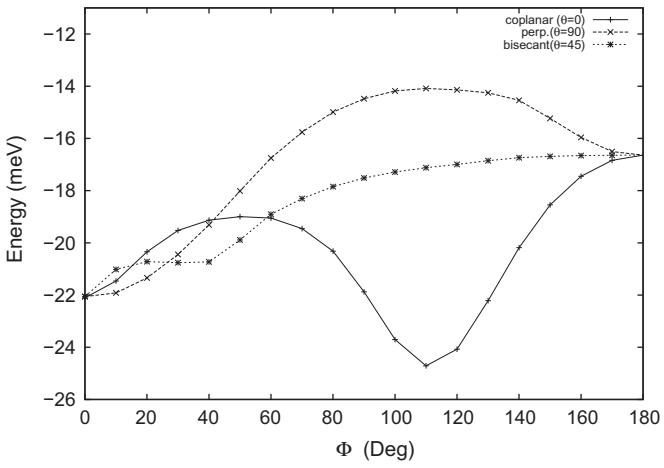

Fig. 5. CCSD (T)/aug-cc-pVQZ optimized interaction energy for Kr–H_2S as a function of Φ (angle between the Kr–S axis and the symmetry axis (C_2) of H_2S). Three different configurations have been reported: coplanar ($\Theta = 0$), the perpendicular ($\Theta = 90$) and bisecant ($\Theta = 45$). See text for details.

To begin comparing the results of the calculations with the experimental observations, which probe a rotational average of the potential and determine a mean well depth ϵ and corresponding equilibrium distance r_m, we can simply average the computed PES parameters, interaction energy and distance, over the angles Θ and Φ of the sections explored. This results in a mean equilibrium distance of 4.13 Å and mean interaction energy of 18.5 meV, which agree remarkably well, in fact within the experimental uncertainty, with the experimental determinations (4.11 Å and 18.8 meV, respectively, see Ref. [16]).

The analysis presented above clearly suggests that the most stable configurations of the H_2S–Kr adduct are those of the coplanar arrangement. A global unconstrained geometry optimization shows indeed that the minimum of the coplanar path seen above is also the absolute minimum of the PES. The results of the geometry optimization with various basis sets are reported in Table 3. They are seen to converge to a distance Kr–S of 3.81 Å and an angle Φ of 111°. The calculation with the largest basis set, aug-cc-pV5Z/CCSD (T), gives a corresponding interaction energy of 25.7 meV. In the table we have also reported the results obtained previously by us [13] at the same level of theory for the H_2O–Kr complex. A very similar pattern of convergence of the results upon increasing the basis set size is observed for both complexes. The H_2S–Kr interaction energy is about 20% larger than that of H_2O–Kr, almost independent of the basis set used. Both systems have the absolute minimum energy configuration in a coplanar arrangement, but the angle of approach of Kr varies substantially by about 50°. Kr approaches water in the neighborhood of an H atom, close to the direction of the corresponding O-H bond (the angle Φ corresponding to an O–H bond is 52.3°). In the case of H_2S–Kr the region of approach of the noble gas is clearly much closer to sulfur. The equilibrium distance Kr–H goes from 2.89 Å in H_2O–Kr to 3.46 Å in H_2S–Kr.

In Fig. 6 we report the optimized distance Kr–S and Kr–O as a function of the angle Φ in the coplanar configuration computed at the same level of theory aug-cc-pVQZ/CCSD (T). The curves follow a qualitatively similar pattern. They show the largest values

Table 3
Computed geometrical parameters of the H_2S–Kr and H_2O–Kr[a] complexes at the CCSD (T) level with different basis sets. r is in Å, Φ is in degrees, E is in meV. All interaction energies are corrected for the BSSE.

	H_2S–Kr			H_2O–Kr[a]		
Basis	r	Φ	E	r	Φ	E
aug-cc-pVDZ	3.91	107	13.1	3.83	62	10.1
aug-cc-pVTZ	3.87	110	21.1	3.78	59	18.0
aug-cc-pVQZ	3.81	111	24.7	3.84	61	20.0
aug-cc-pV5Z	3.81	111	25.7	3.84	62	20.4

[a] Ref. [13].

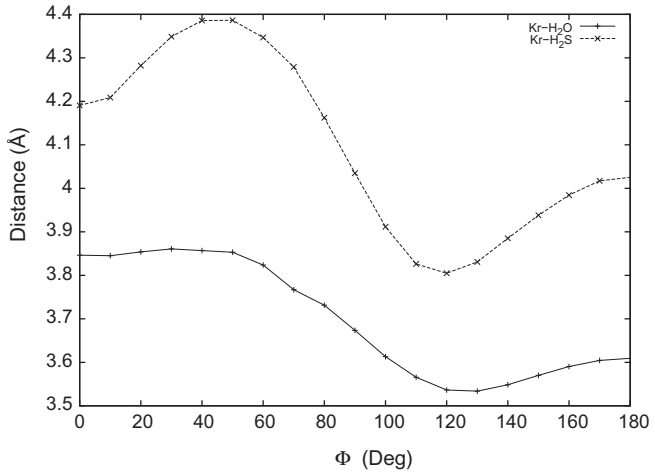

Fig. 6. CCSD (T)/aug-cc-pVQZ optimized distance Kr-X as a function of the angle Φ. X = S,O in H_2S–Kr and H_2O–Kr complexes, respectively.

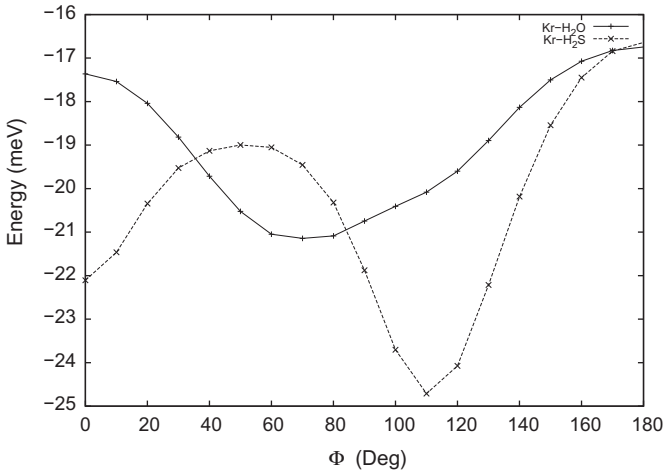

Fig. 7. CCSD (T)/aug-cc-pVQZ optimized energy at the equilibrium distance Kr–O and Kr–S as a function of the angle Φ.

around $\Phi \simeq 40$ degrees while the minimum distance is at much larger values $\Phi \simeq 120$. At $\Phi = 0$ and $\Phi = 180$ both curves present a local minimum and a local maximum, respectively. However, from a more quantitative point of view, the curve of the H_2S–Kr complex shows significantly larger variations, with more pronounced extrema. Indeed, the standard deviation of the distribution of values of r goes from 0.20 Å in the case of H_2S–Kr to almost half that value in H_2O–Kr. It is interesting to note, as the figure also shows, that in the case of H_2O–Kr, the absolute energy minimum ($\Phi = 62°$) lies in the region of the largest r values, while, on the contrary, for H_2S–Kr ($\Phi = 111°$) it is in the region of the closest distances of approach.

In Fig. 7 we compare the coplanar PES sections for both complexes, which clearly look very different. The profile of the H_2S–Kr complex presents four stationary points [40]: two minima at $\Phi = 0$ and $\Phi = 111$ (absolute minimum) and two maxima at about $\Phi = 50$ and $\Phi = 180$. Note that this pattern appears similar to that of the computed S–Kr distance (Fig. 6) discussed above (Fig. 6), suggesting a correlation between larger stabilization energy and closer distance of approach. Such correlation is not observed in the case of the water complex. In fact in this last case only three stationary points can be observed, two local maxima respectively at $\Phi = 0$ and $\Phi = 180$ and the absolute minimum at $\Phi = 62$. This different behavior suggests that a different nature of the interaction may be at work in the two systems, with H_2S–Kr more characterized by van der Waals forces, which are more strictly related to molecular size and thus have a stronger correlation with approach distance. In connection with this, we have recently proved that CT plays a crucial role in the short-range stabilization of the heavier water–Ng complexes. By quantitatively correlating theoretical results and experimental observations, it has been possible to prove for the first time that a small CT (of the order of a couple of me) takes place from the Ng to water [12,13]. Furthermore, it was also found that this CT is a strongly stereoselective and anisotropic phenomenon and that it is mediated by an asymmetric, donor–acceptor, concerted role of the two hydrogen atoms of the

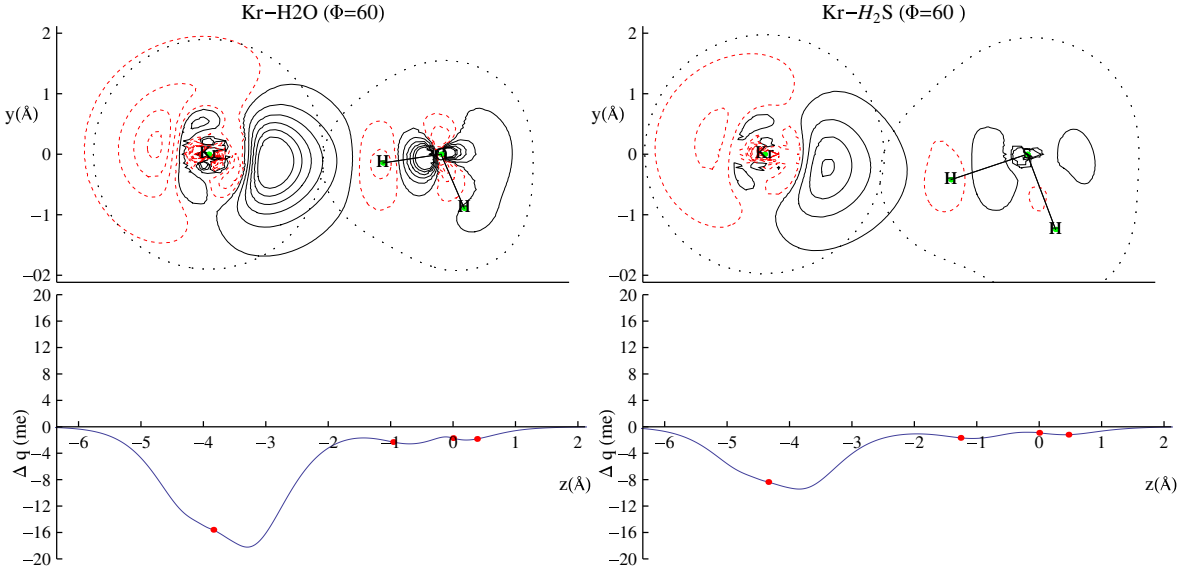

Fig. 8. Contour plots of the electron density changes and $\Delta q(z)$ curves upon formation of the Kr–H_2O and Kr–H_2S binary complexes for $\Phi = 60$. In the contour plots, the dashed lines denote negative values (density depletion) and the solid lines are positive contours. The dotted contours marks the tangent isodensity levels of the isolated fragments. The circles on the Δq curves mark the projection of the nuclear positions on the internuclear axis z (Kr–O axis in the case of water and Kr–S in the case sulfur hydride). The axis origin is at the oxygen position Kr–H_2O and at the sulfur position for Kr–H_2S. See the text for more details.

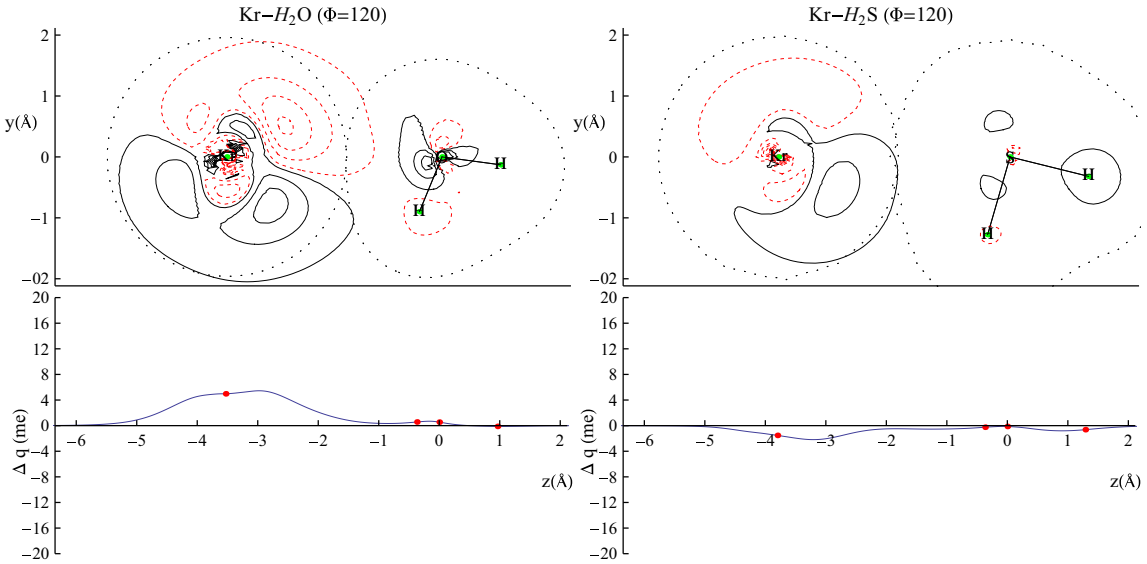

Fig. 9. Contour plots of the electron density changes and $\Delta q(z)$ curves upon formation of the Kr–H_2O and Kr–H_2S binary complexes for $\Phi = 120$. In the contour plots, the dashed lines denote negative values (density depletion) and the solid lines are positive contours. The dotted contours marks the tangent isodensity levels of the isolated fragments. The circles on the Δq curves mark the projection of the nuclear positions on the internuclear axis z (Kr–O axis in the case of water and Kr–S in the case sulfur hydride). The axis origin is at the oxygen position Kr–H_2O and at the sulfur position for Kr–H_2S. See the text for more details.

water molecule, which can in fact dictate the equilibrium geometry of the adducts [12,13]. In the case of the water–Ar complex, we have clearly shown that the CT is maximized in the region where the Ng points in the direction of O–H bond, [12] giving an important contribution at the equilibrium geometry. Water and H_2S have a very similar electronic structure but interacting with the Kr present remarkable differences in the topology of the PES. The question naturally arises what is the role of CT in H_2S–Kr. Is this component peculiar of water interactions or does it occur also in the analogous complexes of H_2S? How do the occurrence and extent of CT generally correlate with the geometry of H_2S–Kr and its PES? More generally, how can one relate the experimental findings with the nature of the interaction? In the following section we attempt to explore these interesting aspects.

5. Charge displacement curves and charge transfer

The key approach in our comparative analysis is the study of the changes in the electron density taking place upon formation of the complexes H_2O–Kr and H_2S–Kr. The electron density change $\Delta\varrho$ is defined as the density difference between the complex and the isolated non-interacting partners placed at the same positions they have in the adducts. (Note that this definition includes the change in density due to the antisymmetrization and renormalization of the total wavefunction made up from the non-orthogonal fragment wavefunctions.) To free our results from any particular theory of charge decomposition, we adopt a scheme based on the definition of charge displacement (CD) along a given axis (z) joining two interacting species, given by

$$\Delta q(z) = \int_{-\infty}^{\infty} dx \int_{-\infty}^{\infty} dy \int_{-\infty}^{z} \Delta\varrho(x,y,z')dz', \qquad (4)$$

where $\Delta\varrho$ is the electron density difference as defined above. Clearly, $\Delta q(z)$ measures, at each point z along the axis, the electron charge that, upon formation of the adduct, is transferred from the right to the left side of the perpendicular plane through z [18]. This approach has been used with success in several contexts [12,14,41]. In the H_2S–Kr and H_2O–Kr system, the z axis is chosen as the axis joining Kr with S and O, respectively. The charge displacement thus defined gives a picture of the direction and extent of electron transfer over the whole inter-fragment space, free of any scheme. The electronic density considered in the following was obtained in all cases at the coupled-cluster level of theory with single and double excitations (CCSD) using the aug-cc-pVQZ basis set. Using this basis set the CD curves are very well converged. A detailed study of the basis set dependence of the CD curves has been presented by us recently for a related system [12].

We start our comparison of the H_2O–Kr and H_2S–Kr complexes considering two geometries that are close to the absolute minima of the corresponding two PESs. The upper panels in Fig. 8 show the contour plots of the electron density difference for the configurations in which Kr approachs water and H_2S, respectively, at an angle $\Phi = 60°$ (close to the angle of minimum energy of H_2O–Kr, $\Phi = 62$). The dotted contours mark the isodensity levels of the isolated fragments that are equal in value and tangent, and may thus be taken as a plausible representation of boundaries enclosing the non-interacting fragments [14]. The lower panels in Fig. 8 report, on the same horizontal scale of the upper plots, the corresponding Δq curves (Eq. 4).

The density deformation contour plots show how the Kr electron cloud is markedly polarized by the presence of water and H_2S. In both cases, there is a lobe of density increase that now extends between the fragments and crosses their boundary. Some charge rearrangement also takes place in the hydride region and there is a small but visible density depletion around the hydrogen atom closer to the approaching Kr. This is accompanied by polarization at the O and S sites, which extends to the far hydrogen. The density pattern is similar in both systems but it is decidedly less pronounced in H_2S–Kr.

The corresponding CD curves immediately make the characterization of the H_2O–Kr and H_2S–Kr interactions in this configuration even clearer. It is, first of all, eye-catching that in both systems the function is negative everywhere. Thus, everywhere in the complexes there is a net CT from left to right, i.e. in the direction going from the Kr towards water or hydrogen sulfide. The curves are qualitatively similar in both complexes but quantitatively different. Electrons flow away from the left side of Kr until a minimum is reached. The CD curves give a clear quantitative measure of such polarization and of the differences between the complexes, showing for instance that, in H_2O–Kr, about 16 millielectrons have

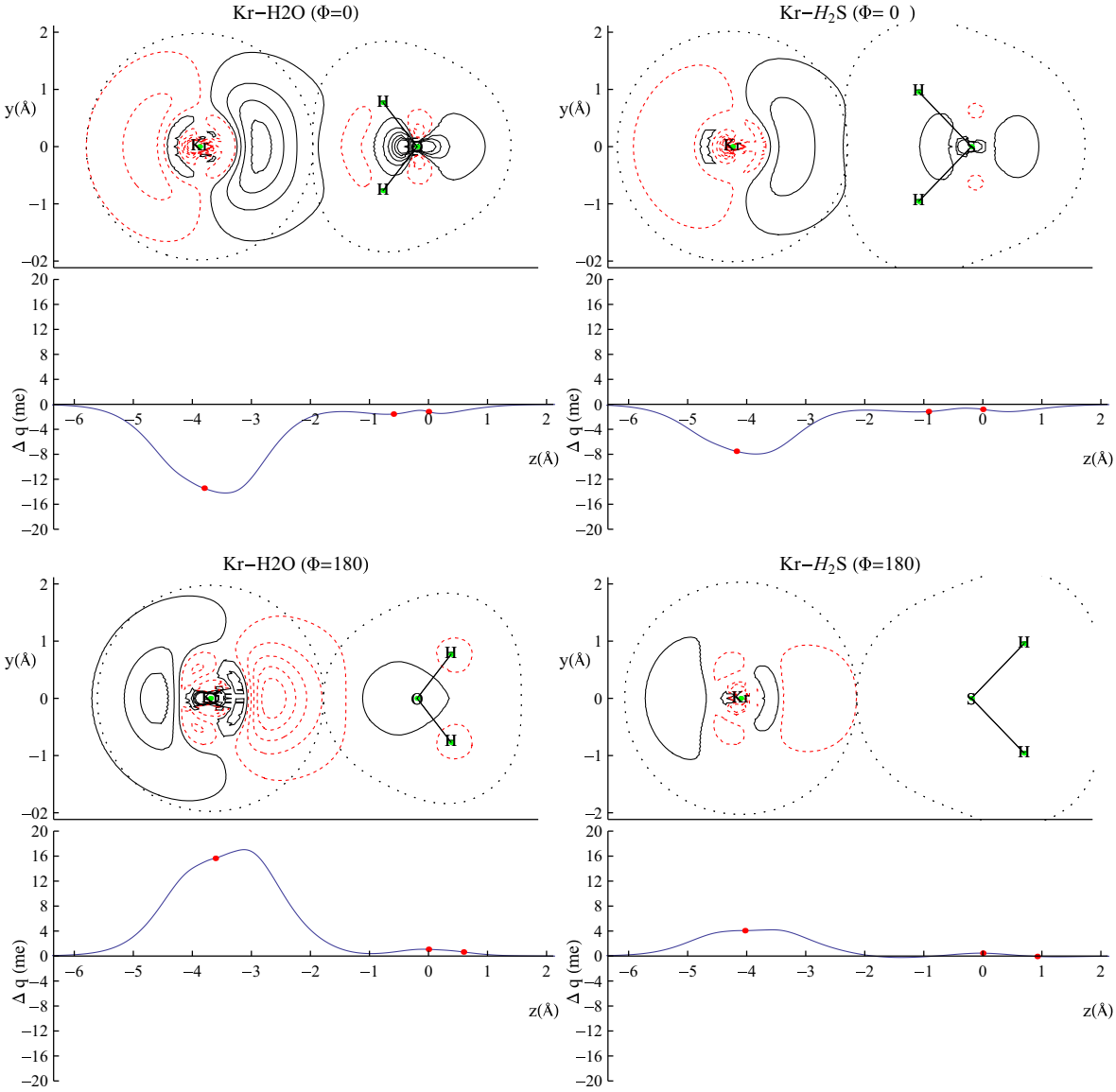

Fig. 10. Contour plots of the electron density changes and $\Delta q(z)$ curves upon formation of the Kr–H_2O and Kr–H_2S binary complexes for $\Phi = 0$ and $\Phi = 180$. In the contour plots, the dashed lines denote negative values (density depletion) and the solid lines are positive contours. The dotted contours marks the tangent isodensity levels of the isolated fragments. The circles on the Δq curves mark the projection of the nuclear positions on the internuclear axis z (Kr–O axis in the case of water and Kr–S in the case sulfur hydride). The axis origin is at the oxygen position Kr–H_2O and at the sulfur position for Kr–H_2S. See the text for more details.

moved from left to right at the site of the Kr, but only about half that amount in the case of H_2S–Kr.

After a minimum the CD curve starts to re-accumulate rapidly until, in the region between the fragments, a maximum (minimum CT magnitude) is found. Let us focus first on the water system. The maximum occurs at 1.8 Å from O, and the value of CT at this point is 1.7 me. This may be considered a lower bound of CT. The CT value at the isodensity boundary between the fragments is a significantly larger 2.9 me. This amount does not vary much going towards water, at least up to the position of the near hydrogen where the CD curve assumes a value of about 2.3 me. A net CT of about 2 me to the right may still be seen even in the region of the far hydrogen atom. But here, in contrast to the region around the left hydrogen, the positive slope of the curve indicates that this hydrogen is an electron acceptor.

The H_2S–Kr complex shows a qualitatively similar patter of CD. The curve maximum is found at about 2 Å from the sulfur position, corresponding to a minimum CT of 1.1 me towards H_2S. The curve is generally flatter than in the water case and, at the isodensity boundary between the fragments, CT is 1.4 me and, again, this amount does not vary significantly further towards hydrogen sulfide. This analysis let us confidently conclude that, in this relative orientation of the fragments, CT is 1.5–2 times larger in the water complex than in the H_2S one.

We consider next, in Fig. 9, the nuclear configuration in which Kr approaches water and H_2S at $\Phi = 120°$, geometry is close to that of the absolute minimum of the H_2S–Kr PES. Here we notice immediately that, in contrast with the previous situation, the qualitative CD patterns in H_2O–Kr and H_2S–Kr differ strikingly. The Kr atom is polarized in opposite directions in the two complexes, with electron density flowing again from left to right of the Kr site in the sulfur adduct but from right to left, and more pronouncedly, in the water one. The CD curve is generally much closer to zero in both cases. However, it is everywhere slightly negative in the H_2S case, indicating again a small CT from Kr to H_2S, while it is positive in H_2O–Kr, indicating that it is water that acts as a weak electron donor in this orientation. Such an inversion in the direction of electron flux with orientation has recently been observed also in the

water–H_2 complex [14]. The CT from Kr to H_2S is seen to stay almost constant at about 0.5 me in a wide region from 1 to 2 Å from S. In the water case, the $H_2O \rightarrow$ Kr electron transfer has a minimum value of about 0.3 me in the inter-fragment region.

In Fig. 10 we have reported the CD analysis for two other interesting stationary points of the coplanar PES, namely $\Phi = 0$ and $\Phi = 180$. Comparison between these shows the effect of orienting the permanent dipole of the hydrides directly towards or away from Kr. At $\Phi = 0$ both complexes show similar contour plots and similar CD curves. Kr exhibits a larger polarization in the water case, where the CD curve is systematically more negative. At the isodensity boundary, CT from Kr is 50% larger to water than to H_2S (1.5 and 1.0 me, respectively). At the opposite orientation, $\Phi = 180°$, Kr polarization (in the other direction) is larger for the water complex, but less pronounced for the H_2S one. The CD curves show that, in the case of water, 16 millielectrons have moved from the left to the right side of the Kr position, about four times the value in H_2S–Kr. This is actually consistent with the expected scaling of the induced dipole on Kr, which goes as the square of the partner's permanent dipole. The permanent dipole of the water is indeed almost twice that of hydrogen sulfide. The CD curve for H_2O–Kr complex is positive across the whole complex region, with a minimum of 0.4 me transferred from water to Kr. The finding of a small but non-negligible water $\rightarrow$ Kr CT is quite interesting, demonstrating that a noble gas may locally accept electrons under the presence of the electric field originating from the permanent dipole moment of water. Note that an analogous CT is not observed in the case of the H_2S–Kr complex where, in fact, the CD curve goes to zero in the region of the isodensity boundary at about 2 Å from the S atom. Interestingly, it was also absent in the H_2O–Ar complex [12], a difference which may be related to the smaller polarizability of the Ar atom compared to Kr. Further studies aimed at investigating these aspects are under way in our laboratory.

6. Summary and conclusions

Integral cross section data $Q(v)$ have been recently measured [13,16] under identical conditions (i.e., high angular and velocity resolution and rotationally "hot" molecular beams) for the whole series of H_2O–Ng and H_2S–Ng systems. Data of the same type are also available for Ng–Ng systems [17]. Their analysis, carried out in an internally consistent way, provided a set of potential parameters whose comparison has allowed us to establish when charge transfer plays an appreciable role and also to evaluate the extent of bond stabilization due to CT. The CT contribution to the interaction is not canceled by the rotational averaging of the colliding molecules. The experimental findings stimulated extensive and accurate theoretical calculations addressed both to the characterization of the full interaction and of the amount and stereoselectivity of CT. In this work we have presented an accurate analysis of several sections of the theoretical PES of H_2S–Kr and compared them with the corresponding profiles of the H_2O–Kr adduct. The most stable adduct geometries have been determined through full geometry optimization and reported here. Contrary to the H_2O–Kr complex, in which the most stable nuclear configuration corresponds to Kr approaching the water molecule towards hydrogen along the direction of an O-H bond, the H_2S–Kr complex prefers a configuration in which Kr lies closer to the sulfur atom.

We have presented a comparative study of the electron density changes accompanying the H_2S–Kr and H_2O–Kr interaction, based on the charge displacement analysis. In most orientations both complexes are found to present a qualitatively similar pattern of CT but this is generally significantly more pronounced (by 50%–150%) in the case of water. In addition, while in H_2S–Kr electron transfer takes place from Kr to the hydride or is absent depending on orientation, water is found to act as a weak electron donor when Kr approaches on the oxygen side. Very interestingly, while in the case of the H_2O–Kr complex the largest CT occurs at the most stable configuration, this is not the case for H_2S–Kr. It may be concluded that CT plays a significant role in governing the interaction involving water [14], while it is less important for H_2S, where van-der-Waals forces dominate. The marginal role of CT in the latter makes it particularly difficult to evaluate experimentally [15,16]. In conclusion, the results of the present investigation constitute an additional important contribution towards a better understanding of the nature of weak interactions involving hydrogenated molecules [42,43].

Acknowledgments

This work was supported by the Italian Ministero dell'Istruzione, Università e Ricerca through PRIN grant no.2008KJX4SN_003.

References

[1] G.C. Maitland, M. Rigby, E.B. Smith, W.A. Wakeham, Intermolecular Forces: Their Origin and determination, Clarendon Press, Oxford, 1987.
[2] A.J. Stone, The Theory of Intermolecular Forces, Oxford University Press, New York, 1996.
[3] G. Desiraju, T. Steiner, The Weak Hydrogen Bond in Structural Chemistry and Biology, Oxford University Press, Oxford, 1999.
[4] P.A. Kollman, L. Allen, Chem. Rev. 72 (1972) 283.
[5] A.E. Reed, L.A. Curtiss, F. Weinhold, Chem. Rev. 88 (1988) 899.
[6] E. Isaacs, A. Shukla, P. Platzman, D. Hamann, B. Barbiellini, C. Tulk, Phys. Rev. Lett. 82 (1999) 600.
[7] J.-H. Guo, Y. Luo, A. Augustsson, J.-E. Rubensson, C. Sathe, H. Agren, H. Siegbahn, J. Nordgren, Phys. Rev. Lett. 89 (2002) 137402.
[8] Official iupac project aimed at categorizing hydrogen-bonding and other intermolecular interactions. <http://www.iupac.org/web/ins/2004-026-2-100>.
[9] A. Stone, A. Mosquitta, Chem. Phys. Lett. 473 (2009) 201.
[10] G.R. Desiraju, Angw. Chem. Int. Ed. 50 (2010) 52.
[11] V. Aquilanti, E. Cornicchi, M. Moix Teixidor, N. Saendig, F. Pirani, D. Cappelletti, Angew. Chemie Int. Ed. 44 (2005) 2356.
[12] L. Belpassi, F. Tarantelli, F. Pirani, P. Candori, D. Cappelletti, Phys. Chem. Chem. Phys. 11 (2009) 9970.
[13] L. Roncaratti, L. Belpassi, D. Cappelletti, F. Pirani, F. Tarantelli, F. Pirani, J. Phys. Chem. A 113 (2009) 15223.
[14] L. Belpassi, M.L. Reca, F. Tarantelli, L.F. Roncaratti, F. Pirani, D. Cappelletti, A. Faure, Y. Scribano, J. Am. Chem. Soc. 132 (37) (2010) 13046.
[15] D. Cappelletti, A.F.A. Vilela, P.R.P. Barreto, R. Gargano, F. Pirani, V. Aquilanti, J. Chem. Phys. 125 (2006) 13311.
[16] V. Aquilanti, D. Cappelletti, F. Pirani, L.F. Roncaratti, Int. J. Mass. Spectr. 280 (2009) 72.
[17] F. Pirani, S. Brizi, L.F. Roncaratti, P. Casavecchia, D. Cappelletti, F. Vecchiocattivi, Phys. Chem. Chem. Phys. 10 (36) (2008) 5489.
[18] L. Belpassi, I. Infante, F. Tarantelli, L. Visscher, J. Am. Chem. Soc. 130 (2008) 1048.
[19] D. Cappelletti, M. Bartolomei, F. Pirani, V. Aquilanti, J. Phys. Chem. A 106 (2002) 10764.
[20] D. Cappelletti, V. Aquilanti, E. Cornicchi, M. Moix-Teixidor, F. Pirani, J. Chem. Phys. 106 (2005) 024302.
[21] E. Luzzatti, F. Pirani, F. Vecchiocattivi, Mol. Phys. 34 (1977) 1279.
[22] V. Aquilanti, G. Liuti, F. Pirani, F. Vecchiocattivi, G.G. Volpi, J. Chem. Phys. 65 (1976) 4751.
[23] T. Nenner, H. Tien, J. Fenn, J. Chem. Phys. 63 (1975) 5439.
[24] F. Pirani, F. Vecchiocattivi, J.J.H. van den Biesen, C.J.N. van den Meijdenberg, J. Chem. Phys. 75 (1981) 1042.
[25] V. Aquilanti, D. Ascenzi, D. Cappelletti, M. de Castro, F. Pirani, J. Chem. Phys. 109 (1998) 3898.
[26] F. Pirani, M. Alberti, A. Castro, M. Moix Teixidor, D. Cappelletti, Chem. Phys. Lett. 394 (2004) 37.
[27] M. Albertí, A. Aguilar, D. Cappelletti, A. Laganà, J.M. Lucas, F. Pirani, Int. J. Mass. Spectr. 280 (2009) 50.
[28] R. Cambi, D. Cappelletti, G. Liuti, F. Pirani, J. Chem. Phys. 95 (1991) 1852.
[29] K. Raghavachari, G.W. Trucks, J.A. Pople, M. Head-Gordon, Chem. Phys. Lett. 157 (1989) 479.
[30] C. Hampel, K.A. Peterson, H.-J. Werner, Chem. Phys. Lett. 190 (1992) 1.
[31] M.J.O. Deegan, P.J. Knowles, Chem. Phys. Lett. 227 (1994) 321.
[32] T.H. Dunning, J. Chem. Phys. 90 (1989) 1007.
[33] D.E. Woon, T.H. Dunning, J. Chem. Phys. 100 (1994) 2975.
[34] D.E. Woon, T.H. Dunning, J. Chem. Phys. 98 (1993) 1358.
[35] H.-J. Werner, P.J. Knowles, R. Lindh, F.R. Manby, M. Schütz, et al., Molpro version 2006.1, a package of ab initio programs. <http://www.molpro.net>.

[36] G. Herzberg, Electronic Spectra and Electronic Structure of Polyatomic Molecules, Van Nostrand, New York, 1966.
[37] G. Tarczay, A.G. Császár, O.L. Polyansky, J. Tennyson, J. Chem. Phys. 115 (3) (2001) 1229.
[38] Y.Z. Song, A.J.C. Varandas, J. Chem. Phys. 130 (13) (2009) 134317.
[39] S.F. Boys, F. Bernardi, Mol. Phys. 19 (1970) 553.
[40] Note that, here and in the following, these stationary points are defined in the reduced dimensionality due to the frozen-geometry of the hydrides.
[41] L. Storchi, L. Belpassi, F. Tarantelli, A. Sgamellotti, H.M. Quiney, J. Chem. Theory Comput. 6 (2) (2010) 384.
[42] P.K. Mandal, D.J. Ramdass, E. Arunan, Chem. Phys. Phys. Chem. 5 (2005) 2740.
[43] M. Goswami, E. Arunan, Chem. Phys. Phys. Chem. 11 (2009) 8974.